

**1 Long tails in regional surface temperature probability
2 distributions with implications for extremes under
3 global warming**

Tyler W. Ruff¹, J. David Neelin^{1,2}

T. W. Ruff, Commodity Weather Group, 4866 Cordell Avenue, Bethesda, MD 20814, USA
(truff@atmos.ucla.edu).

J. D. Neelin, Dept. of Atmospheric and Oceanic Sciences, University of California, Los Angeles,
CA 90095-1565, USA (neelin@atmos.ucla.edu).

¹Department of Atmospheric and Oceanic
Sciences, University of California, Los
Angeles, Los Angeles, California, USA.

²Institute of Geophysics and Planetary
Physics, University of California, Los
Angeles, Los Angeles, California, USA.

4 Prior work has shown that probability distributions of column water va-
5 por and several passive tropospheric chemical tracers exhibit longer-than-
6 Gaussian (approximately exponential) tails. The tracer-advection prototypes
7 explaining the formation of these long-tailed distributions motivate explo-
8 ration of observed surface temperature distributions for non-Gaussian tails.
9 Stations with long records in various climate regimes in National Climatic
10 Data Center Global Surface Summary of Day observations are used to ex-
11 amine tail characteristics for daily average, maximum and minimum surface
12 temperature probability distributions. Each is examined for departures from
13 a Gaussian fit to the core (here approximated as the portion of the distri-
14 bution exceeding 30% of the maximum). While the core conforms to Gaus-
15 sian for most distributions, roughly half the cases exhibit non-Gaussian tails
16 in both winter and summer seasons. Most of these are asymmetric, with a
17 long, roughly exponential, tail on only one side. The shape of the tail has
18 substantial implications for potential changes in extreme event occurrences
19 under global warming. Here the change in the probability of exceeding a given
20 threshold temperature is quantified in the simplest case of a shift in the present-
21 day observed distribution. Surface temperature distributions with long tails
22 have a much smaller change in threshold exceedances (smaller increases for
23 high-side and smaller decreases for low-side exceedances relative to exceedances
24 in current climate) under a given warming than do near-Gaussian distribu-
25 tions. This implies that models used to estimate changes in extreme event

²⁶ occurrences due to global warming should be verified regionally for accuracy
²⁷ of simulations of probability distribution tails.

1. Introduction

28 Understanding the nature of potential changes in the probability of extreme cli-
29 mate/weather events in the context of global warming is vital for future risk manage-
30 ment and assessment of agricultural, economic and ecosystem consequences [*Meehl et al.*,
31 2000; *Parmesan*, 2000; *Christensen et al.*, 2007; *Schlenker and Roberts*, 2009]. There
32 are indications that high extreme temperature anomalies have become more frequent and
33 larger in magnitude in many regions during the past century, and that the occurrence
34 and magnitude of cold extreme anomalies have weakened [*Alexander et al.*, 2006; *Caesar*
35 *et al.*, 2006] although there can be considerable differences among regions or temperature
36 variables such as daily maximum and minimum or extreme cold outbreaks [*Easterling*,
37 2000; *Walsh et al.*, 2001]. Both global and regional scale climate models project changes
38 in the occurrences of temperature extremes under global warming [e.g., *Meehl et al.*, 2007;
39 *Kharin et al.*, 2007; *Christensen et al.*, 2007; *Diffenbaugh et al.*, 2007].

40 As a baseline for a model validation and to gain insight into the natural variability pro-
41 cesses responsible for extreme temperature events, it is useful to examine properties of the
42 tails of the probability distributions in station observations of air temperature. In doing
43 so, there is reason to believe that fine-scale processes will be important [*Diffenbaugh et al.*,
44 2005], suggesting a comparison on local to regional scales. Furthermore, recent observa-
45 tional and theoretical results for transport processes suggest the likelihood of distinct tail
46 properties. Non-Gaussian tails (most of which are approximately exponential) occur very
47 commonly in probability distributions of passive tropospheric chemical tracers and water
48 vapor [*Neelin et al.*, 2010], and their existence is consistent with simple mathematical

49 prototypes for passive tracer advection problems with a forcing that maintains a gradient
50 [e.g., *Bourlioux and Majda, 2002; Pierrehumbert, 2000; Ngan and Pierrehumbert, 2000;*
51 *Majda and Gershgorin, 2010*]. Such long-tailed distributions are hypothesized to occur
52 in near-surface air temperature data since a large portion of near-surface air temperature
53 variability is associated with advection of air masses across a large-scale temperature gra-
54 dient. Although air temperature is not a passive tracer and potentially has complications
55 due to effects of soil moisture [*Diffenbaugh et al., 2007*] and clouds, there is still ample rea-
56 son to expect that probability density functions (PDFs) of temperature might commonly
57 inherit key properties seen in both the observed tracer distributions and the prototypes.
58 Specifically, the tails of the PDF can be longer (often approximately exponential) than
59 would be anticipated from a fit to the core of the PDF (i.e., a central region containing
60 the bulk of the distribution, often approximately Gaussian). We can further anticipate
61 asymmetry in these tails since asymmetry was noted in certain of the observed tracers,
62 and can be easily produced in the prototypes, for instance, if the gradient on the high-
63 tracer side of the region of interest differs from the gradient on the low-tracer side or if
64 the advecting flow has an asymmetry between shorter intense flow events in one direction
65 versus longer, less intense flow events in the other [*Neelin et al., 2010*]. Other effects can
66 also contribute to long tails in geophysical applications related to temperature, including
67 multiplicative noise processes such as a stochastic damping [*Sura and Sardeshmukh, 2008;*
68 *Sura and Perron, 2010*].

69 The influence of tail behavior on the risk of extreme events under global warming
70 underlies the pragmatic importance of quantifying tail characteristics. The commonly

71 stated qualitative explanation [e.g., *Meehl et al.*, 2000, 2007; *Trenberth et al.*, 2007; *Walker*
72 *and Diffenbaugh*, 2008] for changes in extreme events under global warming is of a shift in
73 the mean causing an increase in the frequency of events exceeding a certain threshold value,
74 or conversely a decrease in the occurrences of temperatures below a certain threshold (such
75 as freezing temperature or chill temperature relevant to certain agricultural products).
76 While this overall picture remains, the presence of non-Gaussian tails implies that a
77 change in such distributions can potentially have more complex behavior than that of a
78 pure Gaussian, which can be characterized simply by the mean and standard deviation.
79 A dependence on gradient and flow characteristics in the region of interest is one possible
80 complication suggested by the simple prototypes, so locations in various climate regimes
81 are examined in Section 3. Once the existence of long-tailed behavior is established, as is
82 the aim here, the behavior of the distribution under global warming becomes potentially
83 more complex; relatively simple changes, for instance in zonal wind, potentially alter the
84 properties of such tails [*Majda and Gershgorin*, 2011]. Here we show that even in the
85 simplest case where climate change is assumed to shift the distribution with increasing
86 temperature, the form of the tails has a dramatic impact on the increase of the probability
87 of exceeding a given threshold temperature, as discussed in Section 4.

2. Data and methods

88 The data product used in this paper is the Global Surface Summary of Day (GSOD)
89 version 7, produced by the National Climatic Data Center (NCDC), consisting of 18 daily
90 surface meteorological variables. The input data are derived from the synoptic/hourly
91 observations contained in U.S. Air Force DATSAV3 Surface data and Federal Climate

92 Complex Integrated Surface Data (ISD) [Lott *et al.*, 2008]. Most stations discussed in
93 this paper are from within the United States owing to the relatively long length of the
94 time series, typically spanning from around 1950 through 2009. Effort was made to only
95 include stations with relatively few missing values and no other major data quality issues.
96 Comparison of the GSOD data to the corresponding NCDC Global Historical Climatology
97 Network (GHCN) version 1 daily station data [Peterson and Vose, 1997] at several stations
98 showed no significant differences.

99 The three temperature variables of focus are the daily maximum (T_{\max}), daily average
100 (T_{avg}), and daily minimum (T_{\min}), and the corresponding distributions are shown for each
101 station over JJA (June, July, August) or DJF (December, January, February). To remove
102 potential biases owing to multi-decadal warming or cooling, the time series are linearly
103 detrended. The seasonal cycle is removed by subtracting the daily climatology, calculated
104 as the mean of each calendar day over all years in the time domain (leap days were removed
105 for simplicity), which proved sufficiently smooth due to the long time series considered
106 here.

107 The probability distributions are plotted as histograms using a bin width of $5/9^{\circ}\text{C}$
108 (except where noted otherwise) to prevent artifacts from the conversion from Fahrenheit
109 to Celsius. A Gaussian curve is shown on each distribution for reference. One could
110 define the curve with the standard deviation σ of the entire distribution, but this would
111 be affected by the presence of non-Gaussian tails. Therefore, the Gaussian is fit to the core
112 of the distribution by polynomial regression, which we chose to be all points exceeding
113 a threshold of 0.3 of the distribution maximum. At this threshold, the σ of the core

114 is typically only $\sim 5\text{-}15\%$ less than the value of σ for the entire distribution (with the
115 exception of stations with the most marked tails, e.g., LAX Airport, Los Angeles, CA,
116 Long Beach, CA, and San Juan, Puerto Rico). Lower thresholds decrease this value by
117 a few percent but the fit becomes overly skewed by tails, while higher thresholds rapidly
118 increase the σ difference and tends to inflate the appearance of tails. A few instances were
119 found with departures from Gaussian so marked that even the cores exhibit differences
120 from a Gaussian fit.

121 To assess statistical significance of the tails, an error envelope is created by sampling
122 artificial time series from a Gaussian first-order autoregressive [AR(1)] process that ap-
123 proximates the core. The AR(1) process is chosen to match the standard deviation and
124 1-day autocorrelation time for each station and season. The process fits the observed
125 autocorrelation at lags to at least several days to a week. For each distribution, the error
126 statistic is calculated by simulating 1000 artificial time series the same length as the sta-
127 tion data and computing each of the 1000 histograms as was done for the observations.
128 A confidence interval is constructed using the 5th to 95th percentiles of the spread in
129 each bin. That is, the top of the confidence interval exceeds 95% of the values in each
130 bin constructed from the artificial series using the same time series length and binning
131 procedure.

3. Regional consistencies and differences in probability distributions

132 Figure 1a displays the probability distributions of daily temperature anomalies (after
133 subtracting the climatology and detrending), with the Gaussian core fit and the AR(1)
134 error envelope superimposed, for each of the three variables (T_{\max} , T_{avg} , T_{\min}) during JJA

135 (summer) at the four stations LAX Airport, Los Angeles, CA, Long Beach, CA, Phoenix,
136 AZ, and Houston, TX. Each of the stations exhibits marked departures from Gaussian
137 in at least two of the temperature variables in one of the tails. As expected, asymmetry
138 is common. In each of these stations, one long tail is found, while the other either does
139 not depart strongly from Gaussian or decreases more rapidly than the Gaussian fit to the
140 core. This is common among stations sampled.

141 LAX and Long Beach are chosen primarily to demonstrate the consistency among sta-
142 tions in similar climate configurations (coastal/Mediterranean) in close proximity (within
143 20 km), and both are seen to exhibit long positive tails in T_{\max} and T_{avg} over the summer
144 season. It is apparent that T_{\max} , T_{avg} , and T_{\min} can substantially differ in tail behavior this
145 varies among regions. In the LAX and Long Beach cases, the positive tails in T_{\max} and
146 T_{avg} could be explained by the occasional advection of relatively hot air masses from land,
147 while the absence of strong tails in T_{\min} indicates that the minimum temperature may
148 instead be controlled by the sea breeze and ocean air temperatures. High-side long tails
149 in T_{\max} and T_{avg} are also present in the DJF season for these stations (not shown).

150 The Phoenix and Houston stations, in subtropical arid and subtropical humid climate
151 regimes, respectively, share similar distribution characteristics during JJA. Both are lo-
152 cated in areas close to a local maximum of climatological temperature with little gradient,
153 and thus might be anticipated to exhibit a diminished high-side tail because there is no
154 neighboring region from which to advect a substantially warmer air mass. As discussed
155 in detail in Section 4, the Gaussian (or shorter) nature of the positive tails in these two
156 cities will have different implications under global warming when compared to the roughly

157 exponential tails found in the Los Angeles stations. The Phoenix and Houston stations
158 also exhibit cold side tails in all three variables during summer.

159 Figure 1b displays four stations—Grand Junction, CO, Seattle, WA, Chicago, IL, and
160 Prague, Czech Republic—in the same format as Figure 1a, except for DJF. With the
161 exception of Seattle, these stations represent interior continental climate regimes, and all
162 of which contain distributions with interesting tail configurations during the winter. Non-
163 Gaussian low-side tails exist for at least two temperature variables for these stations, and
164 asymmetry is seen in varying degrees due to the tendency for high-side tails to depart less
165 from the Gaussian. A substantial asymmetry also exists in the cores of the Chicago and
166 Prague stations. The tendency towards a skewed non-Gaussian core is also found in many
167 other stations among all three variables, with the majority of such occurring in DJF and
168 not JJA. Also interesting are the relative contributions of T_{\max} and T_{\min} to T_{avg} —one may
169 expect the average temperature to fall roughly between the maximum and minimum values
170 for a given day, as is evident in most JJA cases. However, T_{avg} seems to mimic T_{\min} in the
171 Grand Junction low-side tail, whereas T_{avg} in Prague exhibits a longer tail relative to the
172 core than either T_{\min} or T_{\max} . Although we display examples of non-Gaussian low-side tails
173 during the winter season in Figure 1b, there are also many stations that do not exhibit
174 such long tails. The regional differences in low-side tail characteristics among stations
175 implies that certain regions are more susceptible to changes in extreme value frequency
176 under global warming, as mentioned for the JJA cases. In these cases, a positive shift
177 in the mean temperature implies a decrease in the occurrences of temperatures below
178 a certain threshold, and the tail characteristics of the distribution will help determine

179 the probability of such a decrease. This may be of practical importance for agricultural
180 products that are sensitive to the freezing or chill temperature.

4. Exceedance thresholds

181 The existence of long tails in temperature distributions—and the differing characteristics
182 among stations—have substantial implications for changes in frequency of extreme tem-
183 perature events over a particular location under gradual shift in mean temperature, as
184 in projected global warming. Implications involving potential changes in tail properties
185 can be addressed in simple prototypes [*Majda and Gershgorin, 2011*] or regional climate
186 models [*Diffenbaugh et al., 2007*]. A class of implications that can be addressed directly
187 from the observed distributions may be inferred for the simplest case where the mean of
188 the distribution is assumed to shift. For advection-dominated tails, this corresponds to
189 assuming that flow statistics and temperature gradient remain constant while the large-
190 scale background temperature increases. If tail characteristics are consequential in this
191 simple case, they appear likely to be at least as important in more complex cases. This
192 simple case can be discussed quantitatively by calculating the increase of the probabil-
193 ity of exceeding a given high-side threshold temperature T_H or the decrease in low-side
194 exceedances (i.e. falling below low-side threshold T_L) under a positive shift ΔT of the
195 mean of the distribution. Another approach [*Kharin and Zwiers, 2005*] fits distributions
196 of extreme occurrences in a given interval that apply asymptotically in the limit of large
197 samples. Here we focus on assessing the potential significance of the tail properties in
198 observed distributions, and of hence the importance of physically interpreting regional

199 disparities. Evidence for the usefulness of a simple shift in describing observed changes is
200 discussed, e.g., in *Simolo et al.* [2010].

201 Figure 2 illustrates the implications of tail properties for a shift of the observed temper-
202 ature anomaly distribution for San Juan, Puerto Rico, which was chosen because it has
203 long tails on both low and high sides permitting both cases to be illustrated for a single
204 station; it also has a clearly defined core and the tails are approximately exponential.
205 Shaded in green in Figure 2a under the positive tail is the region of integration from the
206 threshold temperature T_H up to the maximum nonzero bin of the distribution, represent-
207 ing the climatological probability of exceedance of this threshold. Here the value of T_H is
208 chosen to be 3 standard deviations ($\sim 2.5^\circ\text{C}$ for San Juan) above the mean (denoted as
209 $T_H = 3\sigma$ hereafter). The simplest case of a positive temperature increase is illustrated by
210 shifting the observed distribution by $\Delta T = 1^\circ\text{C}$ ($\sim 0.8\sigma$ for San Juan), with the increased
211 probability of exceedance of T_H indicated by the green region in Figure 2b. The negative
212 tail is integrated from the minimum nonzero bin to $T_L = -3\sigma$ and then shifted by ΔT
213 $= 1^\circ\text{C}$ to obtain a measure of the decrease in frequency of exceedances in this warming
214 scenario.

215 The magnitude of a potential increase in frequency of extreme temperature events oc-
216 ccurring over a particular location in the future will depend on the tail characteristics of
217 the distribution—and will differ strongly from Gaussian tails to long (e.g., approximately
218 exponential) tails. We can quantify this difference between tail types by calculating the
219 ratio of the probability of exceedance of T_H or T_L as a function of the shift ΔT for a given
220 long-tailed distribution and then comparing it to the hypothetical exceedance ratio of the

221 Gaussian fit over the same interval. Figure 2c displays exceedance ratio curves for the
222 positive tail in San Juan for the case of the actual tail (black curve), the approximated
223 exponential tail (red curve), and for the Gaussian fit (blue curve; note that the Gaussian
224 fit characterizing the core is continued through the end of the observable part of the tail
225 region when integrating). Under 1°C warming shift, this ratio for $T_H = 3\sigma$ would increase
226 by about a factor of 30 for the Gaussian fit. However, for the actual positive tail seen in
227 this distribution, seen closely matching the exponential fit, the probability of exceedance
228 increases by less than a quarter of this amount for a 1°C warming and much less rapidly
229 for larger warming. Indeed, extending to a 1.5°C warming would place the Gaussian fit
230 at a factor of about 100 while the actual tail at only 10.

231 Conversely, Figure 2b shows the ratio curves associated with the low-side tail integra-
232 tions decreasing with increasing ΔT , representing the diminishing probability of exceeding
233 the threshold temperature under the warming. The Gaussian ratio curve (blue curve) is
234 seen to be diminishing much more rapidly than the actual curve (black) and the expo-
235 nential fit (red curve): after a 1°C warming, there remains a 30% exceedance probability
236 in the actual exponential tail case, but only a 0.85% probability under the Gaussian fit.

5. Discussion and conclusions

237 Analysis of observational surface temperature probability distributions here finds non-
238 Gaussian tails to be common in station measurements over a range of locations and
239 climate zones. To provide a rough summary statistic for the 29 stations and the three
240 temperature variables (T_{\max} , T_{\min} , and daily average) examined here, approximately half
241 these distributions exhibit substantial departure from Gaussian in the tails on at least one

side (for details see Table A1 and Fig. A1 of the Auxiliary Material). This fraction was similar in summer and winter. Three quarters of the stations had at least one variable qualifying as non-Gaussian in each of JJA and DJF. Only 7% of the stations had tails that were consistent with Gaussian within the sampling error bars for all three temperature variables in both seasons.

Asymmetric distributions are very common among those that depart significantly from Gaussian, with the vast majority having a long tail only on one side (high side or low side depending on location). Similar asymmetry in observed tracers and possible causes have been discussed in *Neelin et al.* [2010]. Overall, these tails appear qualitatively consistent with tracer advection prototypes, but the differences in behavior between minimum, maximum and daily averaged temperature and the differences in distribution among different regions suggest the step from qualitative understanding to quantitative simulation may be significant. For most locations, clear departures from Gaussian were confined to the tails, with the core adequately fit by a Gaussian (to within error bars from a Monte Carlo sampling of a synthetic time series). For a few locations, more severe non-Gaussianity was encountered with departures occurring even within the core (as may be seen for Chicago T_{\min} in Fig. 1b). In a number of cases with strong asymmetry, fits to the core show shorter-than Gaussian tails occurring on one side (as may be seen for some variables in Fig. 1, e.g., for Long Beach, Seattle, Chicago; see also Auxiliary Material). These are not highlighted here because we do not have as clear a prototype from tracer-advection problems for this behavior at this time. However, this behavior and the physical mechanism for it is important to substantiate in future work. Shorter-than-Gaussian tails would

264 have the converse consequences for change of threshold exceedances under global warming
265 than the long-tailed case discussed below, in some cases enhancing risk of strong changes
266 in threshold exceedances.

267 The tail characteristics of regional distributions have a number of potential consequences
268 for threshold exceedances under global warming. While only the simplest case is examined
269 here—that of a large-scale temperature increase causing a shift in mean of the observed
270 distribution—the consequences of tail characteristics are substantial. Locations with high-
271 side tails that are roughly Gaussian, such as Phoenix and Houston, have a much higher
272 increase of exceedances of a high threshold value for a given warming shift than do those
273 with prominent high-side exponential tails, such as coastal Los Angeles. In other words,
274 under a given warming a Gaussian-tailed region tends to be at greater risk of heat wave
275 events that have seldom been encountered than a comparable long-tailed region. In the
276 latter, an increase in heat waves exceeding a given threshold does occur but the region is
277 more likely to have experienced such extremes in the past and thus to have infrastructure
278 which is adapted to such occurrences.

279 The sensitive dependence of tail characteristics on regional effects noted here suggests
280 that it will be (i) useful to understand the physical mechanisms that produce them (includ-
281 ing the observed asymmetry, and the sources of regional dependence); and (ii) essential to
282 verify whether high-resolution models accurately reproduce observed tail characteristics
283 for any region for which an assessment of extreme events is being conducted. A model
284 that has an error in the nature of the tail, e.g., erroneously produces a Gaussian rather

285 than a long tail under current climate for a particular region, will likely have serious errors
286 in quantitatively predicting the increase in exceedances under future climate.

287 **Acknowledgments.** This work was supported in part by National Science Founda-
288 tion grant AGS-1102838 and National Oceanic and Atmospheric Administration grants
289 NA08OAR4310597 and MAPP10689676. The authors thank J.E. Meyerson for assistance
290 with data and graphics.

References

- 291 Alexander, L., Global observed changes in daily climate extremes of temperature and
292 precipitation, *J. Geophys. Res.*, *111*, D05,109, 2006.
- 293 Bourlioux, A., and A. J. Majda, Elementary models with probability distribution function
294 intermittency for passive scalars with a mean gradient, *Physics of Fluids*, *14*, 881–897,
295 2002.
- 296 Caesar, J., L. Alexander, and R. Vose, Large-scale changes in observed daily maximum and
297 minimum temperatures: Creation and analysis of a new gridded data set., *J. Geophys.*
298 *Res.*, *111*, D05,101, 2006.
- 299 Christensen J. H., B. Hewitson, A. Busuioc, A. Chen, X. Gao and coauthors, Regional
300 climate projections, in *Climate Change 2007: The Physical Science Basis. Contribution*
301 *of Working Group I to the Fourth Assessment Report of the Intergovernmental Panel on*
302 *Climate Change*, edited by S. Solomon, D. Qin, M. Manning, Z. Chen, M. Marquis, K. B.
303 Averyt, M. Tignor, H. L. Miller, pp. 847–940, Cambridge University Press, Cambridge,
304 UK, 2007.

- 305 Diffenbaugh, N. S., J. S. Pal, R. J. Trapp, and F. Giorgi, Fine-scale processes regulate
306 the response of extreme events to global climate change, *Proc. Natl. Acad. Sci.*, *102*,
307 15,774–15,778, 2005.
- 308 Diffenbaugh, N. S., J. S. Pal, F. Giorgi, and X. Gao, Heat stress intensification in the
309 mediterranean climate change hotspot, *Geophys. Res. Lett.*, *34*, L11,706, 2007.
- 310 Easterling, D. R., J. L. Evans, P. Y. Groisman, T. R. Karl, K. E. Kunkel, and P. Ambenje,
311 Observed variability and trends in extreme climate events: A brief review, *Bull. Amer.*
312 *Meteor. Soc.*, *81*, 417–425, 2000.
- 313 Kharin, V. V., and F. W. Zwiers, Estimating extremes in transient climate change simu-
314 lations, *J. Climate*, *18*, 1156–1173, 2005.
- 315 Kharin, V. V., F. W. Zwier, and G. C. H. X. Zhang, Changes in temperature and precip-
316 itation extremes in the ipcc ensemble of global coupled model simulations, *J. Climate*,
317 *20*, 1419–1444, 2007.
- 318 Lott, N., R. Vose, S. A. Del Greco, T. F. Ross, S. Worley and J. L. Comeaux, The
319 integrated surface database: Partnerships and progress, *88th AMS Annual Meeting*, 20-
320 25 January 2008, New Orleans, Louisiana, combined preprints, American Meteorological
321 Society, Boston, MA, 2008.
- 322 Majda, A. J., and B. Gershgorin, Quantifying uncertainty in climate change science
323 through empirical information theory, *Proc. Nat. Acad. Sci.*, *107*, 14,958–14,963, 2010.
- 324 Majda, A. J., and B. Gershgorin, Link between statistical equilibrium fidelity and fore-
325 casting skill for complex systems with model error, *Proc. Nat. Acad. Sci.*, *108*, 2011.

- 326 Meehl, G. A., T. F. Stocker, W. D. Collins, P. Friedlingstein, A. T. Gayeand, and coau-
327 thors, Global climate projections, in *Climate Change 2007: The Physical Science Basis.*
328 *Contribution of Working Group I to the Fourth Assessment Report of the Intergovern-*
329 *mental Panel on Climate Change*, edited by S. Solomon, D. Qin, M. Manning, Z. Chen,
330 M. Marquis, K. B. Averyt, M. Tignor, H. L. Miller, pp. 747–845, Cambridge University
331 Press, Cambridge, UK, 2007.
- 332 Meehl, G. A., W. D. Collins, B. A. Boville, J. T. Kiehl, T. M. L. Wigley, and J. M.
333 Arblaster, Response of the NCAR climate system model to increased CO₂ and the role
334 of physical processes, *J. Climate*, *13*, 1879–1898, 2000.
- 335 Neelin, J. D., B. R. Lintner, B. Tian, Q. Li, L. Zhang, P. K. Patra, M. T. Chahine, and
336 S. N. Stechmann, Long tails in deep columns of natural and anthropogenic tropospheric
337 tracers, *Geophys. Res. Lett.*, *37*, L05,804, 2010.
- 338 Ngan, K., and R. T. Pierrehumbert, Spatially correlated and inhomogeneous random
339 advection, *Physics of Fluids*, *12*, 822–834, 2000.
- 340 Parmesan, C., T. L. Root, and M. R. Willig, Impacts of extreme weather and climate on
341 terrestrial biota, *Bull. Amer. Meteor. Soc.*, *81*, 443–450, 2000.
- 342 Peterson, T., and R. Vose, An overview of the global historical climatology network tem-
343 perature database, *Bull. Amer. Meteor. Soc.*, *78*, 2837–2849, 1997.
- 344 Pierrehumbert, R. T., Lattice models of advection-diffusion, *Chaos*, *10*, 61–74, 2000.
- 345 Schlenker, W., and M. J. Roberts, Nonlinear temperature effects indicate severe damages
346 to us crop yields under climate change, *Proc. Natl. Acad. Sci.*, *106*, 15,594–15,598, 2009.

- 347 Simolo, C., M. Brunetti, M. Maugeri, T. Nanni, and A. Speranza, Understanding climate
348 change-induced variations in daily temperature distributions over Italy, *J. Geophys.*
349 *Res.*, *115*, D22,110, 2010.
- 350 Sura, P., and M. Perron, Extreme events and the general circulation: Observations and
351 stochastic model dynamics, *J. Atmos. Sci.*, *67*, 2785–2804, 2010.
- 352 Sura, P., and P. D. Sardeshmukh, A global view of non-Gaussian SST variability, *J.*
353 *Physical Oceanography*, *38*, 639–647, 2008.
- 354 Trenberth K. E., P. D. Jones, P. Ambenje, R. Bojariu, D. Easterling, and coauthors,
355 Observations: Surface and atmospheric climate change., in *Climate Change 2007: The*
356 *Physical Science Basis. Contribution of Working Group I to the Fourth Assessment*
357 *Report of the Intergovernmental Panel on Climate Change*, edited by S. Solomon, D.
358 Qin, M. Manning, Z. Chen, M. Marquis, K. B. Averyt, M. Tignor, H. L. Miller, pp.
359 235–336, Cambridge University Press, Cambridge, UK, 2007.
- 360 Walker, M., and N. Diffenbaugh, Evaluation of high-resolution simulations of daily-scale
361 temperature and precipitation over the United States, *Clim. Dyn.*, *33*, 1131–1147, 2008.
- 362 Walsh, J. E., A. S. Phillips, D. H. Portis, and W. L. Chapman, Extreme cold outbreaks
363 in the United States and Europe, *J. Climate*, *14*, 2642–2658, 2001.

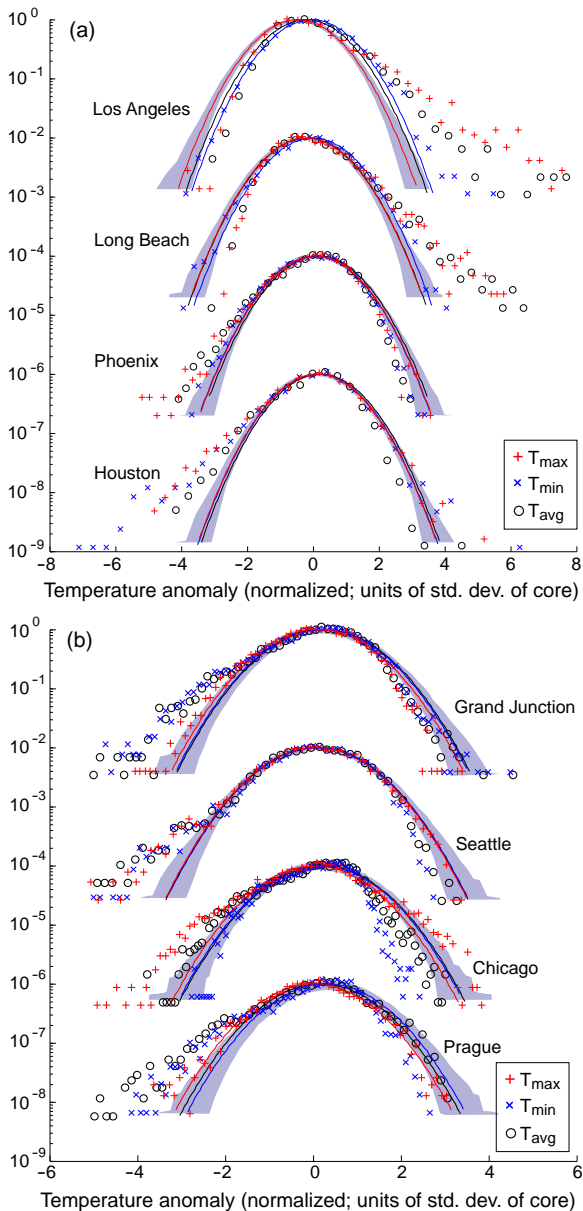


Figure 1. (a) Probability distributions (as normalized frequency of occurrence) of daily temperature anomalies, normalized by the standard deviation of a Gaussian fit to the core (fit for points exceeding 30% of the maximum, drawn as solid lines), at selected stations (vertically shifted for clarity) during JJA (summer). Stacked for each station are the variables T_{\max} (red), T_{avg} (black), and T_{\min} (blue). The shaded error envelope (from sampling artificial autocorrelated Gaussian time series as described in Section 2) is shown for T_{\max} at each station (the envelopes for T_{avg} and T_{\min} are very similar). (b) As in (a) but for during DJF (winter), and the error envelope is shown for T_{\min} at each station.

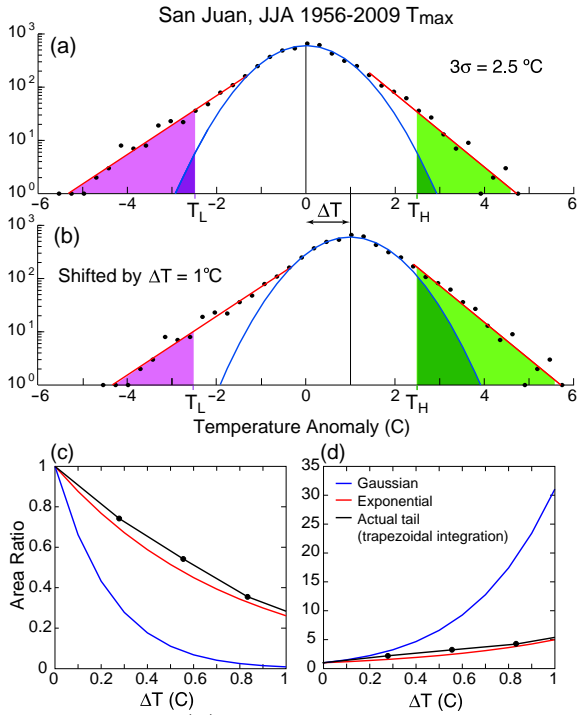


Figure 2. (a) Probability distribution function (shown as frequency of occurrence) for anomalies of daily maximum surface air temperature at San Juan, Puerto Rico (black dots). The blue curve shows a Gaussian core fit to values above 30% of maximum; the red lines show exponential fits to the low-side and high-side tails. The regions representing exceedances of a threshold value $T_H = 3\sigma = 2.5^\circ\text{C}$, on the high side, or $T_L = -3\sigma$ on the low side, are shown in green and purple respectively (dark shading for the corresponding region if the tails followed the Gaussian fit to the core). Exceedance probabilities are integrated between T_H or T_L and the furthest bin with nonzero values in the respective tails (note shaded regions are not area proportional on this log plot). (b) Ratio of the probability of low-side exceedance of T_L as a function of the shift ΔT of the distribution to probability in the un-shifted case, comparing this ratio for the observed tail (black), for an exponential fit to the tail (red) and for a continuation of the Gaussian corresponding to the core (using the same integration interval as for the observations). (c) As in (b), but for the high-side case.